micromachines

Article

Improvement of Single Event Transient Effects for a Novel AlGaN/GaN High Electron-Mobility Transistor with a P-GaN Buried Layer and a Locally Doped Barrier Layer

Juan Xiong [1,†], Xintong Xie [2,†], Jie Wei [2], Shuxiang Sun [1,2,*] and Xiaorong Luo [2,3,*]

[1] Henan Key Laboratory of Smart Lighting, School of Information Engineering, Huanghuai University, Zhumadian 463000, China
[2] State Key Laboratory of Electronic Thin Films and Integrated Devices, University of Electronic Science and Technology of China, Chengdu 610054, China
[3] College of Microelectronics, Chengdu University of Information Technology, Chengdu 610225, China
* Correspondence: sunshuxianga@126.com (S.S.); xrluo@uestc.edu.cn (X.L.)
† These authors contributed equally to this work.

Abstract: In this paper, a novel AlGaN/GaN HEMT structure with a P-GaN buried layer in the buffer layer and a locally doped barrier layer under the gate (PN-HEMT) is proposed to enhance its resistance to single event transient (SET) effects while also overcoming the degradation of other characteristics. The device operation mechanism and characteristics are investigated by TCAD simulation. The results show that the peak electric field and impact ionization at the gate edges are reduced in the PN-HEMT due to the introduced P-GaN buried layer in the buffer layer. This leads to a decrease in the peak drain current (I_{peak}) induced by the SET effect and an improvement in the breakdown voltage (BV). Additionally, the locally doped barrier layer provides extra electrons to the channel, resulting in higher saturated drain current ($I_{\mathrm{D,sat}}$) and maximum transconductance (g_{max}). The I_{peak} of the PN-HEMT (1.37 A/mm) is 71.8% lower than that of the conventional AlGaN/GaN HEMT (C-HEMT) (4.85 A/mm) at 0.6 pC/μm. Simultaneously, $I_{\mathrm{D,sat}}$ and BV are increased by 21.2% and 63.9%, respectively. Therefore, the PN-HEMT enhances the hardened SET effect of the device without sacrificing other key characteristics of the AlGaN/GaN HEMT.

Keywords: GaN HEMT; single event transient (SET) effect; P-GaN buried layer; locally doped barrier layer

Citation: Xiong, J.; Xie, X.; Wei, J.; Sun, S.; Luo, X. Improvement of Single Event Transient Effects for a Novel AlGaN/GaN High Electron-Mobility Transistor with a P-GaN Buried Layer and a Locally Doped Barrier Layer. *Micromachines* **2024**, *15*, 1158. https://doi.org/10.3390/mi15091158

Academic Editor: Parsian K. Mohseni

Received: 20 August 2024
Revised: 12 September 2024
Accepted: 13 September 2024
Published: 16 September 2024

1. Introduction

In recent years, high electron-mobility transistors (HEMTs) based on GaN/AlGaN heterostructures have made significant progress due to their excellent material properties, including high electron mobility, a high electric field strength, a wide bandgap, and more [1–4]. With the continuous improvement of microelectronics fabrication techniques, the current gain cutoff frequency (f_{T}) and maximum oscillation frequency (f_{max}) of GaN HEMTs have greatly increased [5–7], making them highly suitable for aerospace and satellite power applications [8–10].

When GaN HEMTs are used in space equipment, their operating characteristics can be limited by irradiation effects. One of the most common radiation effects is the single event transient (SET) effect caused by high-energy heavy ions in space [11–13], which can alter the operating state of the device and even lead to permanent damage. To date, the SET effects in GaN HEMTs have been extensively studied by many researchers [14–17]. The high impact ionization rate in the high electric field region of GaN HEMTs results in the generation of more electron–hole pairs, leading to a significant increase in electron collection by the drain electrode and, consequently, increased sensitivity to SET effects [18,19]. Therefore, one method to improve the radiation hardness of GaN HEMTs against SET effects is to reduce the electric field. To modulate the electric field distribution, a gate field plate is commonly utilized [20–22]. However, the field plate will induce additional parasitic gate capacitance, decaying the f_T and f_{max} of the device. Introducing a P-type buried layer structure is an effective method to modulate the channel electric field and has been reported by many researchers [23–26]. A dual-channel P-type buried layer has been used to decrease the electric field near the drain channel, resulting in an increase in single-event burnout voltage for GaN MISFETs [27]. However, the P-type buried layer reduces the electron concentration in the channel, leading to the degradation of GaN HEMT characteristics. Therefore, a method that reduces the sensitivity of the device to SET effects without sacrificing other characteristics is needed.

In this work, to enhance the SET hardening and DC characteristics of GaN HEMTs, a novel HEMT with a p-GaN buried layer in the buffer layer and a locally doped barrier layer under the gate (PN-HEMT) is proposed and investigated by TCAD simulation. It was observed that the peak drain current (I_{peak}) induced by the SET effect in the PN-HEMT is significantly decreased due to the P-GaN buried layer. The I_{peak} of the PN-HEMT is 71.8% lower than that of the conventional HEMT (C-HEMT). Furthermore, it was found that the saturated drain current ($I_{D,sat}$) of the PN-HEMT is slightly increased by 21.2% compared with that of the C-HEMT, due to the locally doped barrier layer.

2. Device Structure and Simulation Details

Figure 1a shows the structure of the PN-HEMT. A P-GaN buried layer in the buffer layer and a locally doped barrier layer under the gate are the notable features of the PN-HEMT. The simulations are carried out in Sentaurus TCAD [28], and physics models are introduced, such as the DopingDep and High-field dependent mobility model, the piezoelectric polarization (strain) model, the impact ionization model, and the Schockley–Read–Hall recombination model. The length and thickness of locally doped $Al_{0.3}Ga_{0.7}N$ barrier are 2.1 µm and 20 nm, respectively. The doping concentration of the locally doped $Al_{0.3}Ga_{0.7}N$ barrier is 1×10^{18} cm^{-3}. The distance from the P-GaN buried layer to the GaN channel (D) is 50 nm and the thickness of the P-GaN buried layer is 0.1 µm. The doping concentration of the P-GaN buried layer is 7×10^{17} cm^{-3}. Figure 1b shows the structure of the C-HEMT. The work function of gate is set as 5.2 eV to model the Ni/Au Schottky contact of the actual device [29]. The other parameters are shown in Table 1.

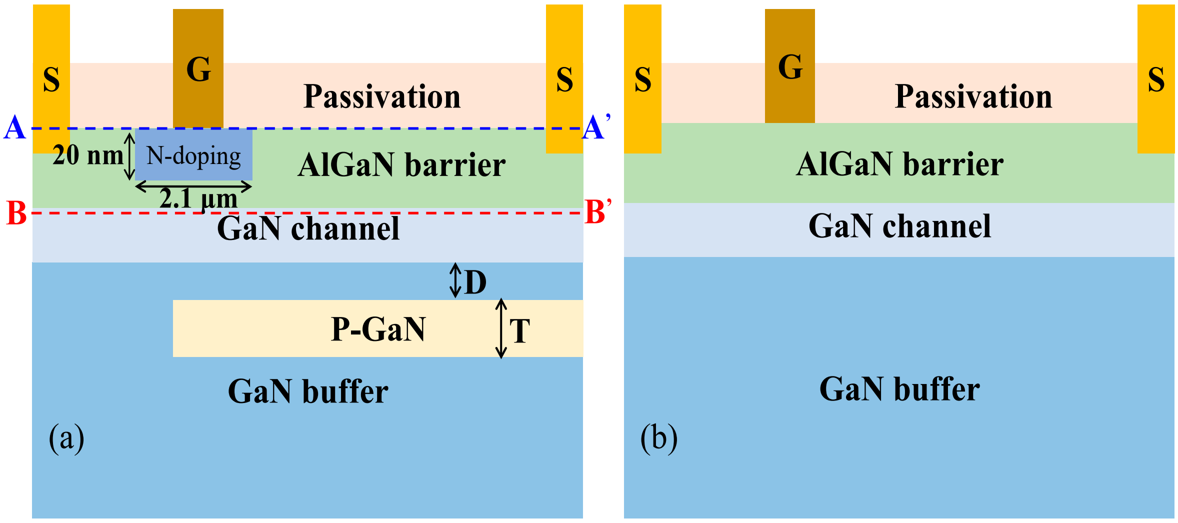

Figure 1. Schematic cross-section of (**a**) PN-HEMT and (**b**) C-HEMT.

Table 1. Parameters of the PN-HEMT in simulation.

Parameter	Value
$Al_{0.3}Ga_{0.7}N$ barrier layer thickness	25 nm
GaN channel layer thickness	100 nm
Thickness of P-GaN buried layer (T)	100 nm
Distance from channel for P-GaN buried layer (D)	50 nm
P-GaN layer doping concentration (N_P)	7×10^{17} cm^{-3}
GaN buffer layer thickness	1.4 µm
Gate–source spacing	1.4 µm
Gate–drain spacing	2.4 µm

To investigate the SET performance of the devices, the HeavyIon model is adopted. Under the harshest conditions, the incidence position of the particle is set at the gate edge closest to the drain [19,26], with the particle traveling vertically across the device. After the particle strike, the generation rate of electron–hole pairs is described by a spatial and temporal Gaussian function, which is expressed as follows [30,31]:

$$rate(x,t) = \frac{LET}{q\pi\omega_0 T_C} \exp\left[-\frac{(x-x_0)^2}{{\omega_0}^2}\right] \cdot \exp\left[-\frac{(t-T_0)^2}{{T_C}^2}\right] \tag{1}$$

where the spatial Gaussian function width ω_0 and the temporal Gaussian function width T_C are set as 0.06 µm and 5×10^{-12} s, respectively. The initial time T_0 of the charge generation is set to 2×10^{-11} s. The LET value in simulation is 0.6 pC/µm, which corresponds to 63.8 MeV·cm^2/mg for Ta [32], with a conversion factor of 0.0095 [33].

3. Results and Discussion

3.1. Basic Characteristics

Figure 2 illustrates the DC characteristics of the PN-HEMT, C-HEMT, N-HEMT (with only the locally doped barrier layer), and P-HEMT (with only the P-GaN buried layer). The results show that a much higher saturated drain current ($I_{D,sat}$) and maximum transconductance (g_{max}) are achieved for the N-HEMT and PN-HEMT. This improvement is attributed to the locally doped barrier layer in the proposed structures. In the PN-HEMT and N-HEMT, the locally doped barrier layer provides additional electrons to the channel, thereby enhancing electron density from the x-coordinate at the gate's right-side edge to the locally doped barrier's right-side edge [34], as shown in the dashed pink box in Figure 3. Consequently, a much higher $I_{D,sat}$ is observed for the N-HEMT and PN-HEMT. Moreover, the lowest $I_{D,sat}$ is observed in the P-HEMT, as the buried P-GaN island partially depletes the 2DEG. Compared to the $I_{D,sat}$ and g_{max} of 591 mA/mm and 254 mS/mm in the C-HEMT, a higher $I_{D,sat}$ of 716 mA/mm and g_{max} of 267 mS/mm are achieved in the PN-HEMT.

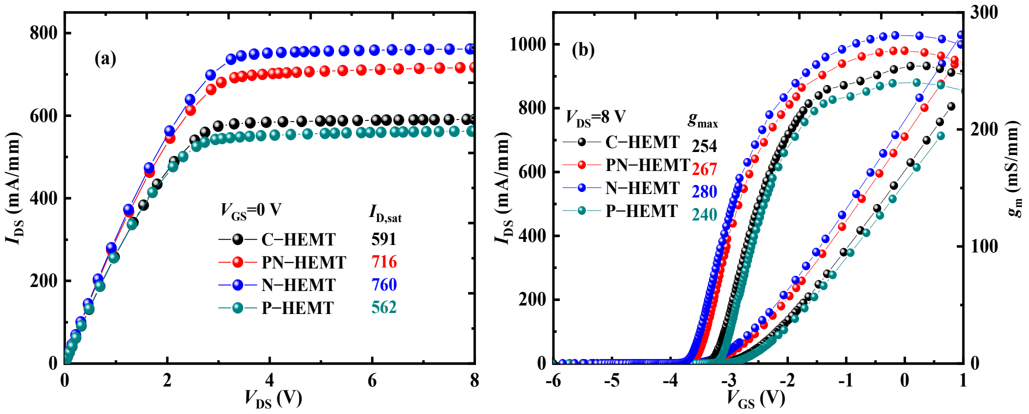

Figure 2. (**a**) Output and (**b**) transfer characteristics for different devices.

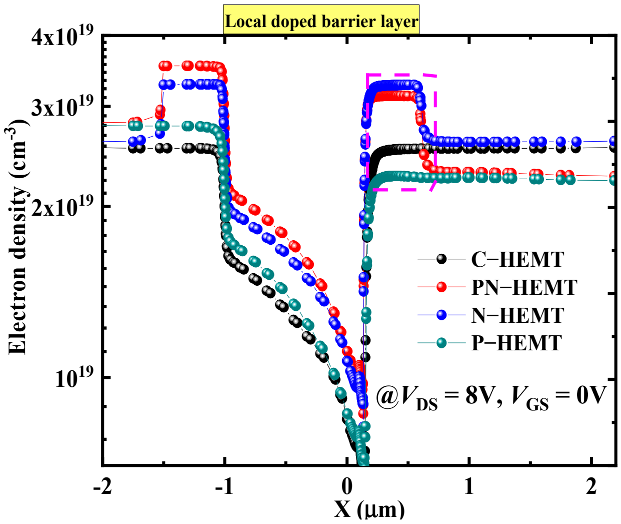

Figure 3. Electron concentration along the channel for different devices.

Figure 4a compares the I−V characteristics of the PN-HEMT and C-HEMT. The breakdown voltage (BV) is extracted from the $I_{DS}-V_{DS}$ curve when I_{DS} = 1 mA/mm. Compared to the BV of 289 V in the C-HEMT, a higher BV of 800 V is achieved by the proposed PN-HEMT. Figure 4b,c show the distribution of equipotential lines for the PN-HEMT and C-HEMT at breakdown. As shown in Figure 4b, the equipotential lines are more uniformly distributed between the gate and drain owing to the redistribution of the electric field of the P−GaN buried layer [35,36]. However, the equipotential lines for the C-HEMT are more crowded near the gate. Additionally, the buffer leakage current is reduced by the P−GaN buried layer, further increasing the BV. Consequently, the PN-HEMT achieves a higher BV.

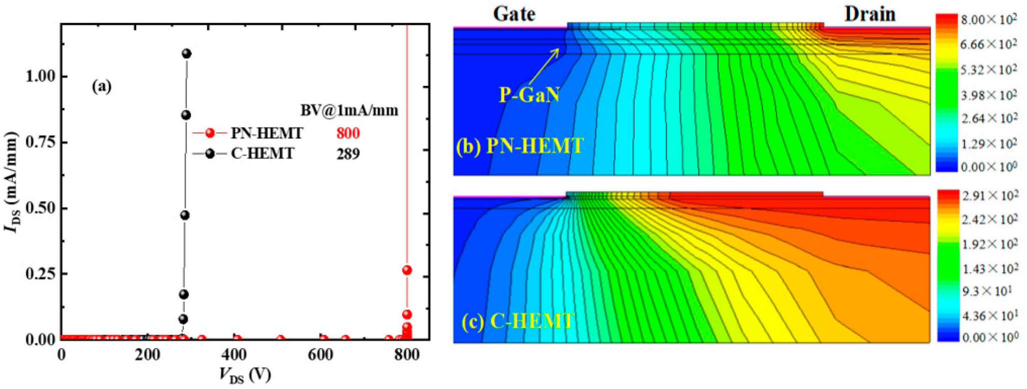

Figure 4. (**a**) I–V characteristics curves and (**b**,**c**) distribution of equipotential lines at breakdown.

3.2. SET Effect

The variations in I_{DS} over time for the PN-HEMT and C-HEMT after a particle strike at V_{DS} = 50 V and V_{GS} = −6 V (off state) are shown in Figure 5. After the particle strike, the I_{DS} for both devices initially increase rapidly and reach their peaks (I_{peak}), then quickly decrease. The I_{peak} of the PN-HEMT (1.37 A/mm) is 71.8% lower than that of the C-HEMT (4.85 A/mm). Additionally, the drain current pulse duration of the PN-HEMT is shorter than that of the C-HEMT. Therefore, the PN-HEMT demonstrates a much better resistance to the SET effect compared to the C-HEMT.

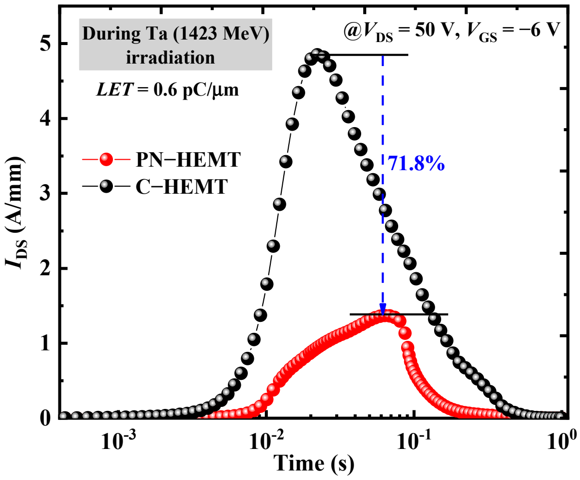

Figure 5. Drain currents as a function of time after heavy ion strike (V_{DS} = 50 V and V_{GS} = −6 V).

To explain the lower I_{peak} for the PN-HEMT, the electron density in the channel (BB′) for the PN-HEMT and C-HEMT at peak time is analyzed, as shown in Figure 6a. It can be seen that, due to the P-GaN buried layer depleting electrons in the channel between the gate and drain in the PN-HEMT, there is a noticeable reduction in electron density. In addition, the effect on electron concentration from the locally doped barrier layer under the gate is minimal. However, the electron density remains high in the C-HEMT. To further elucidate the low electron concentration in the PN-HEMT, the impact ionization rate (IR) for the PN-HEMT and C-HEMT at peak time is analyzed, as shown in Figure 6b. The results show that the IR at the AlGaN barrier (AA′) and GaN channel (BB′) interface for the PN-HEMT is smaller than that of the C-HEMT. This is mainly due to the lower electric field along the particle incident path in the PN-HEMT, as shown in Figure 7, which suppresses electron–hole pair ionization. Hence, fewer electrons are generated in the PN-HEMT at peak time, resulting in a significantly lower I_{peak}.

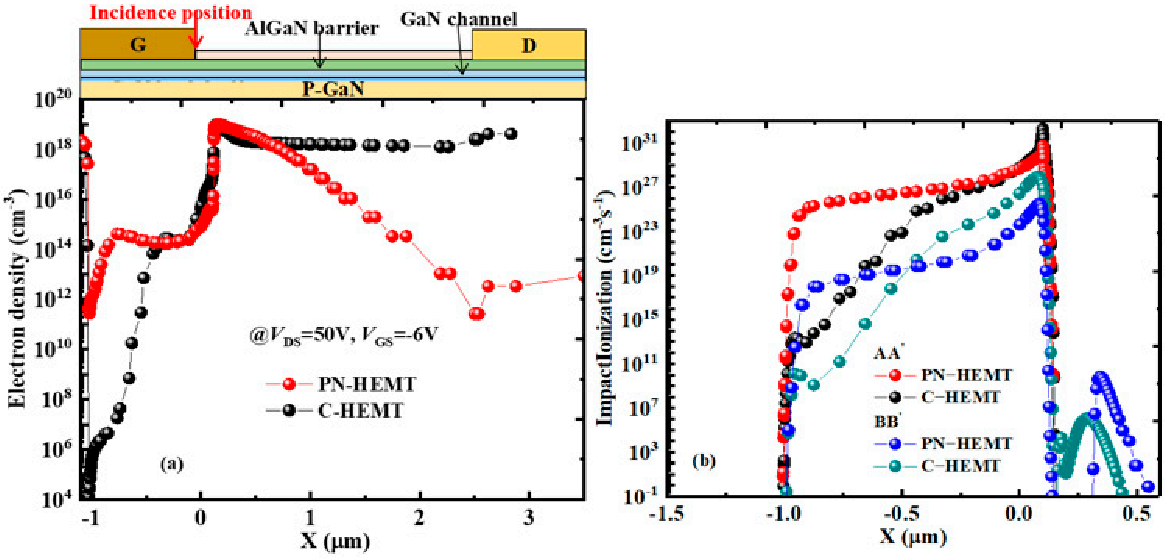

Figure 6. (**a**) Channel electron density distribution (along the line BB′) and (**b**) impact ionization rate for PN-HEMT and C-HEMT at peak time.

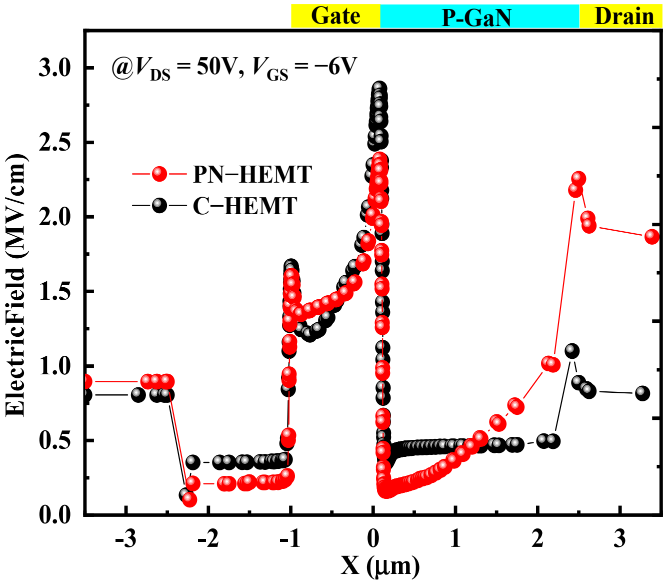

Figure 7. Electric field distribution (along the line BB′) at peak time.

In addition, the P-GaN buried layer increases the SRH recombination rate, as shown in Figure 8, resulting in more electrons being recombined before they are collected by the drain electrode. Consequently, the I_{peak} of the PN-HEMT is further decreased.

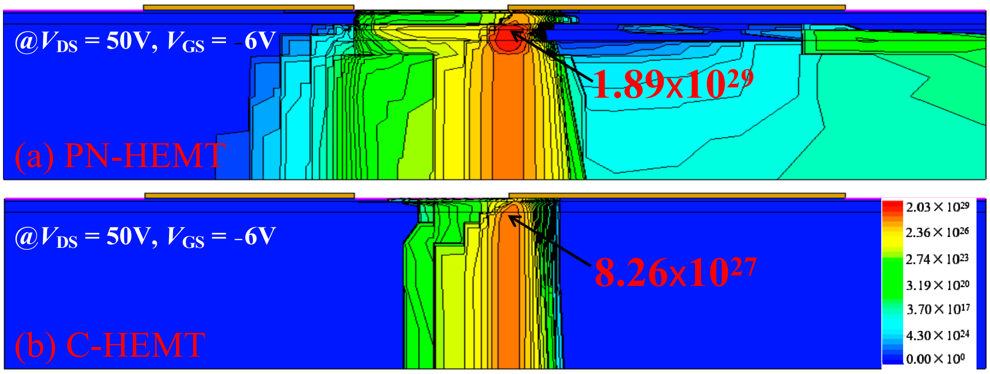

Figure 8. SRH recombination rate at peak time for (**a**) PN-HEMT and (**b**) C-HEMT.

The influences of D and N_P on the I_{peak} of the PN-HEMT at T = 0.05 μm are shown in Figure 9a. The results indicate that the I_{peak} of the PN-HEMT decreases to a minimum and then increases again with the increase in D and N_P. Figure 9b shows the effects of T on the I_{peak}. As T increases, the I_{peak} initially decreases and then increases. This is mainly due to the higher electric field that is obtained with the thicker T, as shown in Figure 10. Changes in the electric field in the device have an important effect on the IR. Therefore, the IR is higher for the thicker T, as shown in Figure 11, and therefore more electron–hole pairs will be generated at a thicker T, resulting in a higher I_{peak}. When N_P is 7 × 10^{17} cm^{-3}, T is 0.1 μm, and D is 0.05 μm, the I_{peak} of the PN-HEMT reaches its lowest value (1.37 A/mm). Simultaneously, $I_{D,\text{sat}}$ and BV are increased by 21.2% and 63.9%, respectively. Therefore, the PN-HEMT enhances the device's resistance to SET effects without sacrificing other key characteristics of the GaN HEMT.

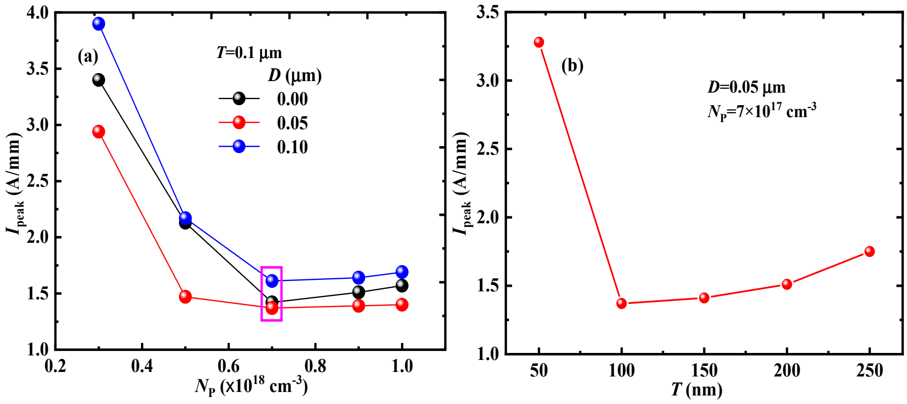

Figure 9. (**a**) Optimized D and N_p and (**b**) T and corresponding I_peak.

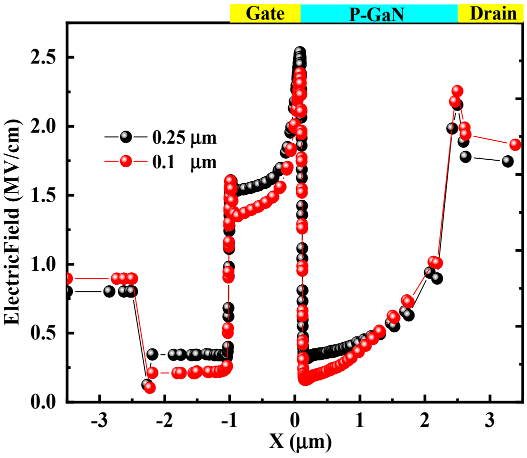

Figure 10. Electric field distribution for different T at peak time.

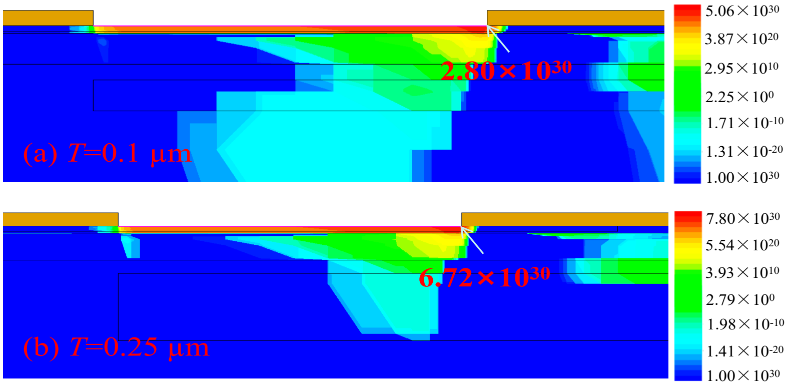

Figure 11. Impact ionization rate for PN-HEMT with different T at peak time.

Figure 12 illustrates the key feasible fabrication process flows for the PN-HEMT. The steps start with epitaxially growing GaN buffer and P-GaN layers on a Si substrate by MOCVD in Figure 12a. The realization of an epitaxial P-GaN layer could be achieved by using Mg as dopant. The P-GaN layer is selectively etched by ICP until the GaN buffer is exposed, as shown in Figure 12b, and, then, surface treatment is used to improve the surface quality [37]. The GaN buffer/GaN channel/AlGaN/N^+-AlGaN are regrown by MOCVD, as shown in Figure 12c [38]. The ICP is utilized to selectively etch N+-AlGaN until the AlGaN layer is exposed, as shown in Figure 12d, which is followed by surface treatment. Subsequently, the regrowth of the AlGaN layer is achieved by MOCVD and a SiN_x passivation layer is formed by LPCVD, as shown in Figure 12e. Afterwards, digital etching is used to form the source and drain trenches, as shown in Figure 12f.

The Ti/Al/Ni/Au stack is deposited with a low-temperature Ohmic process and lift-off for source and drain electrode are performed, as shown in Figure 12g. Finally, the gate electrode is formed by e-beam evaporation after selectively removing SiN_x by RIE, and is then lifted off, as shown in Figure 12h.

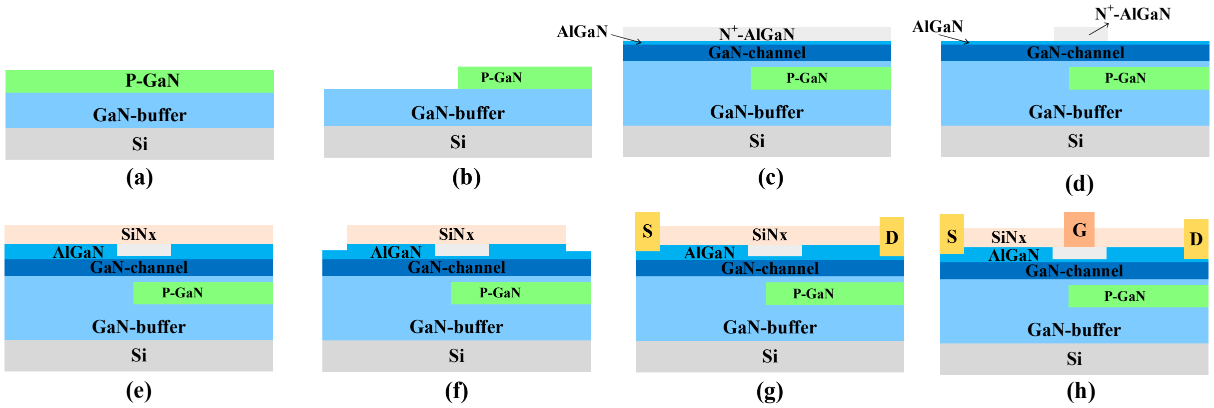

Figure 12. Key fabrication process steps for PN-HEMT.

4. Conclusions

In this paper, a novel HEMT with a P-GaN buried layer in the buffer layer and a locally doped barrier layer under the gate is proposed to enhance resistance to SET effects. The results show that the I_{peak} of the PN-HEMT is significantly decreased due to the reduction in the E_{peak} and IR by the P-GaN buried layer, while the BV is also improved. In addition, the locally doped barrier layer provides extra electrons to the channel, enhancing electron density, resulting in a much higher $I_{D,sat}$ for the PN-HEMT. Consequently, compared to the I_{peak} of 4.85 A/mm in the C-HEMT, the novel PN-HEMT achieves an I_{peak} of 1.37 A/mm, a reduction of 71.8%. The $I_{D,sat}$ and BV of the PN-HEMT are increased to 716 mA/mm and 800 V, respectively, from 591 mA/mm and 289 V in the C-HEMT, representing increases of 21.2% and 63.9%, respectively.

Author Contributions: Conceptualization, X.L. and S.S.; methodology, J.W.; validation, J.W., X.L. and S.S.; formal analysis, X.X.; investigation, X.X. and J.X.; data curation, X.X.; writing—original draft preparation, X.X. and J.X.; writing—review and editing, X.L. and S.S.; funding acquisition, S.S. All authors have read and agreed to the published version of the manuscript.

Funding: This work was supported by the Science and Technology Innovation Key R&D Program of Chongqing under Grant 2024TIAD-STX0009, the Henan Province Joint Fund Project of Science and Technology under Grant 225200810085, Henan Provincial Science and Technology Research Project under Grant 232102210173, 232102320131, the Henan Key Laboratory of Smart Lighting Grant 2023KF07, the Zhumadian City Science and Technology Innovation Youth Project under Grant QNZX202325, the Young Backbone Teacher of Project of Henan Province under Grant 2024GGJS128, the and Young Backbone Teacher of Project of Huanghuai University.

Data Availability Statement: Data are contained within the article.

Conflicts of Interest: The authors declare no conflicts of interest.

References

1. Tian, K.; Zhao, P.; Du, J.; Yu, Q. Design optimization of wide-gate swing E-mode GaN HEMTs with junction barrier Schottky gate. *J. Phys. D Appl. Phys.* **2024**, *57*, 415107. [CrossRef]
2. Liu, H.X.; Huang, H.M.; Wang, K.; Xie, Z.J.; Wang, H. Impact of composition and thickness of step-graded AlGaN barrier in AlGaN/GaN heterostructures. *Mater. Sci. Semicond. Process.* **2024**, *178*, 108460. [CrossRef]
3. Cheng, J.J.; Wang, Q.Y.; Liu, Y.K.; Ding, G.; Zhang, M.M.; Yi, B.; Huang, H.M.; Yang, H.Q. Study on a p-GaN HEMT with composite passivation and composite barrier layers. *Semicond. Sci. Technol.* **2024**, *39*, 085004. [CrossRef]
4. Liu, A.-C.; Huang, Y.-W.; Chen, H.-C.; Kuo, H.-C. Improvement Performance of p-GaN Gate High Electron-Mobility Transistors with GaN/AlN/AlGaN Barrier Structure. *Micromachines* **2024**, *15*, 517. [CrossRef] [PubMed]

5. Husna Hamza, K.; Nirmal, D.; Augustine Fletcher, A.S.; Ajayan, J.; Natarajan, R. Enhanced drain current and cut off frequency in AlGaN/GaN HEMT with BGaN back barrier. *Mater. Sci. Eng. B* **2022**, *284*, 115863. [CrossRef]
6. He, Y.W.; Zhang, L.; Cheng, Z.; Li, C.C.; He, J.H.; Xie, S.J.; Wu, X.K.; Wu, C.; Zhang, Y. Scaled InAlN/GaN HEMT on Sapphire With f_T/f_{max} of 190/301 GHz. *IEEE Trans. Electron. Device* **2023**, *70*, 3001–3004. [CrossRef]
7. Lv, R.P.; Sun, H.Q.; Yang, L.F.; Liu, Z.; Zhang, Y.H.; Li, Y.; Huang, Y.; Guo, Z.Y. Improving RF characteristic and suppress gate leakage in normally-off GaN-HEMTs using negative polarization effect and floating gate for millimeter-wave systems. *Results Phys.* **2024**, *59*, 107526. [CrossRef]
8. Mounika, B.; Ajayan, J.; Bhattacharya, S.; Nirmal, D. Recent developments in materials, architectures and processing of AlGaN/GaN HEMTs for future RF and power electronic applications: A critical review. *Micro Nanostruct.* **2022**, *168*, 207317. [CrossRef]
9. Zerarka, M.; Austin, P.; Bensoussan, A.; Morancho, F.; Durier, A. TCAD Simulation of the Single Event Effects in Normally-OFF GaN Transistors After Heavy Ion Radiation. *IEEE Trans. Nucl. Sci.* **2017**, *64*, 2242–2249. [CrossRef]
10. Mounika, B.; Ajayan, J.; Bhattacharya, S. An intensive study on effects of lateral scaling and gate metals on the RF/DC performance of recessed T-gated Fe-doped AlN/GaN/SiC HEMTs for future RF and microwave power applications. *Microelectron. Eng.* **2023**, *271–272*, 111948. [CrossRef]
11. Nelson, T.; Georgiev, D.G.; Hontz, M.R.; Khanna, R.; Ildefonso, A.; Koehler, A.D.; Hobart, A.; Khachatrian, A.; McMorrow, D. Examination of Trapping Effects on Single-Event Transients in GaN HEMTs. *IEEE Trans. Nucl. Sci.* **2023**, *70*, 328–335. [CrossRef]
12. Li, K.; Hao, J.H.; Zhao, Q.; Zhang, F.; Dong, Z.W. Simulation of heavy ion irradiation effect on 3D MOSFET. *AIP Adv.* **2023**, *13*, 025143. [CrossRef]
13. Liu, B.J.; Li, C.; Chen, M.H. Investigation of Single Event Transient Induced by Process Variability in 14 nm High-k/Metal Gate SOI FinFET Devices. *Silicon* **2023**, *15*, 1317–1324. [CrossRef]
14. Wu, W.R.; Xu, W.T.; Qu, K.; Yang, G.G.; Yu, Z.X.; Sun, W.F. Comprehensive investigation on different ions of geostationary orbitinduced single event burnout in GaN HEMT power devices. *Microelectron. Reliab.* **2023**, *149*, 115187. [CrossRef]
15. Zhang, X.; Cao, Y.; Chen, C.; Wu, L.; Wang, Z.; Su, S.; Zhang, W.; Lv, L.; Zheng, X.; Tian, W.; et al. Study on Single Event Effects of Enhanced GaN HEMT Devices under Various Conditions. *Micromachines* **2024**, *15*, 950. [CrossRef]
16. Liang, Y.; Chen, R.; Han, J.; Wang, X.; Chen, Q.; Yang, H. The Study of the Single Event Effect in AlGaN/GaN HEMT Based on a Cascode Structure. *Electronics* **2021**, *10*, 440. [CrossRef]
17. Das, S.; Kumari, V.; Sehra, K.; Gupta, M.; Saxena, M. TCAD Based Investigation of Single Event Transient Effect in Double ChannelAlGaN/GaN HEMT. *IEEE Trans. Device Mater. Reliab.* **2021**, *21*, 416–423. [CrossRef]
18. Zhen, Z.X.; Feng, C.; Wang, Q.; Niu, D.; Wang, X.L.; Tan, M.Q. Single Event Burnout Hardening of Enhancement Mode HEMTs With Double Field Plates. *IEEE Trans. Nucl. Sci.* **2021**, *68*, 2358–2366. [CrossRef]
19. Khachatrian, A.; Buchner, S.; Koehler, A.; Affouda, C.; McMorrow, D.; LaLumondiere, S.D.; Dillingham, E.C.; Bonsall, J.P.; Scofield, A.C.; Brewe, D.L. The Effect of the Gate-Connected Field Plate on Single-Event Transients in AlGaN/GaN Schottky-Gate HEMTs. *IEEE Trans. Nucl. Sci.* **2019**, *66*, 1682–1687. [CrossRef]
20. Zhang, N.Q.; Keller, S.; Parish, G.; Heikman, S.; DenBaars, S.P.; Mishra, U.K. High breakdown GaN HEMT with overlapping gate structure. *IEEE Electron. Device Lett.* **2000**, *21*, 421–423. [CrossRef]
21. Saito, W.; Nitta, T.; Kakiuchi, Y.; Saito, Y.; Tsuda, K.; Omura, I.; Yamaguchi, M. Suppression of dynamic on-resistance increase and gate charge measurements in high-voltage GaN-HEMTs with optimized field-plate structure. *IEEE Trans. Electron. Device* **2007**, *54*, 1825–1830. [CrossRef]
22. Medjdoub, F.; Derluyn, J.; Cheng, K.; Leys, M.; Degroote, S.; Marcon, D.; Visalli, D.; Van Hove, M.; Germain, M.; Borghs, G. Low on-resistance high-breakdown normally off AlN/GaN/AlGaN DHFET on Si substrate. *IEEE Electron. Device Lett.* **2010**, *31*, 111–113. [CrossRef]
23. Luo, X.; Wang, Y.; Hao, Y.; Cao, F.; Yu, C.H.; Fei, X.X. TCAD Simulation of Breakdown-Enhanced AlGaN-/GaN-Based MISFET with Electrode-Connected p-i-n Diode in Buffer Layer. *IEEE Trans. Electron. Device* **2018**, *65*, 476–482. [CrossRef]
24. Du, J.F.; Liu, D.; Zhao, Z.Q.; Bai, Z.Y.; Li, L.; Mo, J.H.; Yu, Q. Design of high breakdown voltage GaN vertical HFETs with p-GaN buried buffer layers for power switching applications. *Superlattices Microstruct.* **2015**, *83*, 251–260. [CrossRef]
25. Fei, X.; Wang, Y.; Luo, X.; Bao, M.; Yu, C. TCAD simulation of abreakdown-enhanced double channel GaN metal-insulator-semiconductorfield-effect transistor with a P-buried layer. *Semicond. Sci. Technol.* **2020**, *35*, 065012.
26. Wang, Y.; Bao, M.; Cao, F.; Tang, J.; Luo, X. Technology Computer Aided Design Study of GaN MISFET with Double P-Buried Layers. *IEEE Access* **2019**, *7*, 87574–87581. [CrossRef]
27. Fei, X.; Wang, Y.; Sun, B.; Xing, J.; Wei, W.; Li, C. Simulation study of single-event burnout in hardened GaN MISFET. *Radiat. Phys. Chem.* **2023**, *213*, 111244. [CrossRef]
28. Sabui, G.; Parbrook, P.J.; Arredondo-Arechavala, M.; Shen, Z.J. Modeling and simulation of bulk gallium nitride power semiconductor devices. *Aip Adv.* **2016**, *6*, 055006. [CrossRef]
29. Jia, Y.; Wang, Q.; Chen, C.; Feng, C.; Li, W.; Jiang, L.; Xiao, H.; Wang, Q.; Xu, X.; Wang, X. Simulation of a Parallel Dual-Metal-Gate Structure for AlGaN/GaN High-Electron-Mobility Transistor High Linearity Applications. *Phys. Status Solidi A* **2021**, *218*, 2100151. [CrossRef]
30. Yu, C.H.; Guo, H.M.; Liu, Y.; Wu, X.D.; Zhang, L.D.; Tan, X.; Han, Y.C.; Ren, L. Simulation study on single-event burnout in field-plated Ga2O3 MOSFETs. *Microelectron. Reliab.* **2023**, *149*, 115227. [CrossRef]

31. Wang, K.; Wang, Z.; Cao, Y.; Liu, H.; Chang, W.; Zhao, L.; Mei, B.; Lv, H.; Zeng, X.; Xue, Y. Study of the mechanism of single event burnout in lateral depletion-mode Ga_2O_3 MOSFET devices via TCAD simulation. *J. Appl. Phys.* **2024**, *135*, 145702. [CrossRef]
32. Olson, B.D.; Ingalls, J.D.; Rice, C.H.; Hedge, C.C.; Cole, P.L.; Duncan, A.R.; Armstrong, S.E. Leakage Current Degradation of Gallium Nitride Transistors Due to Heavy Ion Tests. In Proceedings of the IEEE Radiation Effects Data Workshop (REDW), Boston, MA, USA, 3 December 2015.
33. Weatherford, T.R. Radiation effects in high speed III-V integrated circuits. *Int. J. High. Speed Electron. Syst.* **2003**, *13*, 277–292. [CrossRef]
34. Fu, W.; Xu, Y.; Yan, B.; Zhang, B.; Xu, R. Numerical simulation of local doped barrier layer AlGaN/GaN HEMTs. *Superlattices Microstruct.* **2013**, *60*, 443–452. [CrossRef]
35. Luo, J.; Zhao, S.; Lin, Z.; Zhang, J.; Ma, X.; Hao, Y. Enhancement of Breakdown Voltage in AlGaN/GaN High Electron Mobility Transistors Using Double Buried p-Type Layers. *Chin. Phys. Lett.* **2016**, *33*, 067301. [CrossRef]
36. Luo, X.; Wang, Y.; Cao, F.; Yu, C.; Fei, X. A breakdown enhanced AlGaN/GaN MISFET with source connected P-buried layer. *Superlattices Microstruct.* **2017**, *112*, 517–527. [CrossRef]
37. Kodama, M.; Sugimoto, M.; Hayashi, E.; Soejim, N.; Ishiguro, O.; Kanechika, M.; Itoh, K.; Ueda, H.; Uesugi, T.; Kachi, T. GaN-Based Trench Gate Metal Oxide Semiconductor Field-Effect Transistor Fabricated with Novel Wet Etching. *Appl. Phys. Express* **2008**, *1*, 021104. [CrossRef]
38. Arifin, P.; Sutanto, H.; Sugianto; Subagio, A. Plasma Assisted MOCVD Growth of Non-Polar GaN and AlGaN on Si(111) Substrates Utilizing GaN-AlN Buffer Layer. *Coatings* **2022**, *12*, 94. [CrossRef]